

CLEAR-SKY BROADBAND IRRADIANCE: FIRST MODEL ASSESSMENT IN URUGUAY

Agustín Laguarda^{1,2}, Gonzalo Abal^{1,2}

1 Laboratorio de Energía Solar/CENUR LN, UDELAR, Salto (Uruguay)

2 Instituto de Física/Facultad de Ingeniería, UDELAR, Montevideo (Uruguay)

Summary

Three simple clear-sky models using easily available mean average atmospheric data are evaluated against hourly ground data for five sites in Uruguay. The ESRA model, based on a mean daily cycle Linke Turbidity calculated from independent GHI ground data, is the best model. It predicts clear-sky irradiance with typical uncertainties under 5 % and bias under 1 % of the average GHI for all sites considered. This is low enough for it to be useful in automatic quality check procedures for ground data and also as a basis for all-sky irradiance estimation based on satellite information.

Key-words: clear-sky irradiance, GHI, Linke Turbidity

1. Introduction

An accurate determination of clear-sky Global Horizontal Irradiation (GHI) is important both as a basis for satellite-based GHI estimation (Cano et al. 1986, Pérez et al. 2002, Rigollier et al. 2004, Pérez et al. 2015) and for automatized data quality assessment. Detailed clear-sky models, such as REST2 (Gueymard, 2008), require accurate data on the state of the atmosphere to achieve their full potential. This information has a local character and is not available at most locations worldwide. Broadband clear-sky models that can perform well using easily available average information, obtained either from ground data or from satellite-based estimates, are considered and evaluated here.

Comparisons between clear-sky models have been performed for several locations worldwide (Gueymard 2012, Reno et al., 2012, Ineichen 2006). However, since both the quality of the available data and the climatic tendencies are location-dependent, the problem of choosing the best clear-sky model must be locally addressed. The review by (Gueymard 2012) provides a useful listing of eighteen clear-sky models with their inputs explicitly listed. They range from zero to eight inputs in the case of REST2, one of the most sophisticated models. Acceptable models for clear-sky GHI have deviations under 6 % of the mean irradiation, the exact figure depending also on the quality of the data and the input parameters. In this work, we present a first inter-comparison between three simple hourly clear-sky models with a few daily-averaged inputs tested against quality-controlled hourly ground data from several sites in the territory of Uruguay, South America.

2. Models, methodology and data

2.1 Clear-sky models

Three models whose input parameters can be determined either from ground-based global horizontal irradiance (GHI) measurements or from reliable satellite-based estimates are considered: (i) the clear sky model used in the European Solar Radiation Atlas, ESRA (Rigollier et al., 2000), (ii) the model proposed in (Ineichen and Perez 2002) based on Kasten's pirheliometric formula (Kasten 1996) and (iii) the simplified version of the SOLIS model proposed in (Ineichen, 2008). The first two rely on a single dimensionless parameter, the Linke Turbidity (TL) for air mass 2 and the third requires mean water vapor density (w) and mean Aerosol Optical Depth at 700 nm ($aod700$). In this work, we refer to these models as ESRA, KIP and

sSOLIS, respectively. In all cases, the corrected air mass m (considering diffraction and altitude effects) and the solar zenith angle are calculated for the mid-point of each hour. The parametrization in (Kasten y Young, 1989) is used for the corrected air mass. A brief description of each of these models is provided here for completeness.

ESRA model: This model (Rigollier et al. 2000) estimates the direct and diffuse irradiance over an horizontal plane, and then adds them to obtain GHI. The Linke Turbidity for an air mass equal to 2 is its single parameter. In its hourly version, the beam component is given by

$$I_{bh}^{ESRA} = I_0 f_n \cos \theta_z e^{-0.8662 m \delta_R T_L} \quad (1)$$

where $I_0 = 1367 \text{ Wh/m}^2$ is the hourly solar constant, $f_n = (r_0/r)^2$ is the orbital eccentricity factor parametrized in (Spencer 1971), and δ_R is the Rayleigh optical thickness (Kasten, 1996). The solar zenith angle, θ_z , is calculated at the midpoint of each hour from location and time information, in the usual form. Further corrections regarding altitude effects according to (Remund, 2003) are not implemented, since all the locations considered are in altitudes over the sea level below 140 meters, and these effects are negligible. The numerical factor 0.8662 in eq. (1) has an historical origin, associated to changes in the parametrization of δ_R . In early work, the Rayleigh optical thickness parametrization did not include absorption by permanent gases in the atmosphere and these effects appeared as an increased effective turbidity (Inechien y Perez, 2002; Mavromatakis y Franghiadakis, 2007). In later work (Louche et al., 1986; Grenier et al., 1994; Kasten, 1996) the parametrization of δ_R was modified to include these effects and consequently, the turbidity $T_L(m)$ was adjusted, since the product $\delta_R(m) \cdot T_L(m)$ is independent of air mass. The ratio of Linke Turbidity (new/old) at $m=2$ gives rise to the 0.8662 factor in eq. (1) (Kasten, 1996). The Linke Turbidity coefficient takes into account the effects due to water vapor and aerosols and it is frequently interpreted as the number of clear, dry atmospheres which would produce the same effect on solar radiation as the actual atmosphere.

Diffuse irradiation on a horizontal plane is estimated as the product of the extraterrestrial irradiation times a diffuse transmittance factor on a vertical path (T_z) multiplied by a diffuse angular modifier F_d ,

$$I_{dh}^{ESRA} = I_0 f_n T_z(T_L) F_d(\theta_z, T_L) \quad (2)$$

The T_z and F_d expressions proposed in (Rigollier, 2000) are used here. Localization of this part of the model can be done with diffuse irradiation data. However, under clear sky conditions the diffuse fraction in the region of interest is about 10% (Abal et al. 2017), so small deviations due to the diffuse parametrization are expected to have little impact on model performance. The sum of eq. (1) and eq. (2) then provide the global irradiation on a horizontal surface.

KIP model: A second clear-sky model based on Linke Turbidity is described in (Kasten, 1984). Inechien and Perez observed a solar zenith angle and altitude dependence in its performance and introduced a correction (Inechien and Perez, 2002) which implies the inclusion of two altitude-dependent parameters a_1 and a_2 and the parametrization of global horizontal irradiation as ,

$$I_h^{KIP} = a_1 I_0 f_n \cos \theta_z e^{-a_2 m [f_{h1} + f_{h2} (T_L - 1)]} \quad (3)$$

Here $f_{h1} = \exp(-h/8000)$ and $f_{h2} = \exp(-h/1250)$ are coefficients that depend on the site altitude above sea level (h) in meters. The KIP model introduces a_1 and a_2 as linear functions of the altitude (Inechien and Perez, 2002) so that at sea level ($h=0$) a version of Kasten's original model is obtained. However in this formulation T_L is the main parameter used to describe the atmosphere.

sSOLIS Model: This simplified version of the SOLIS model, adequate for real-time use, has been proposed by (Inechien, 2008). The original SOLIS model is a spectrally resolved physical model based on radiative transfer model (RTM) calculations. The empirical equation is adopted as a good approximation for GHI,

$$I_h^{sSOLIS} = I_0' f_n \cos \theta_z e^{-\frac{\tau_g}{\cos^g \theta_z}} \quad (4)$$

Similar expression are used for beam and diffuse irradiance. I_0' is an enhanced extraterrestrial irradiance. In

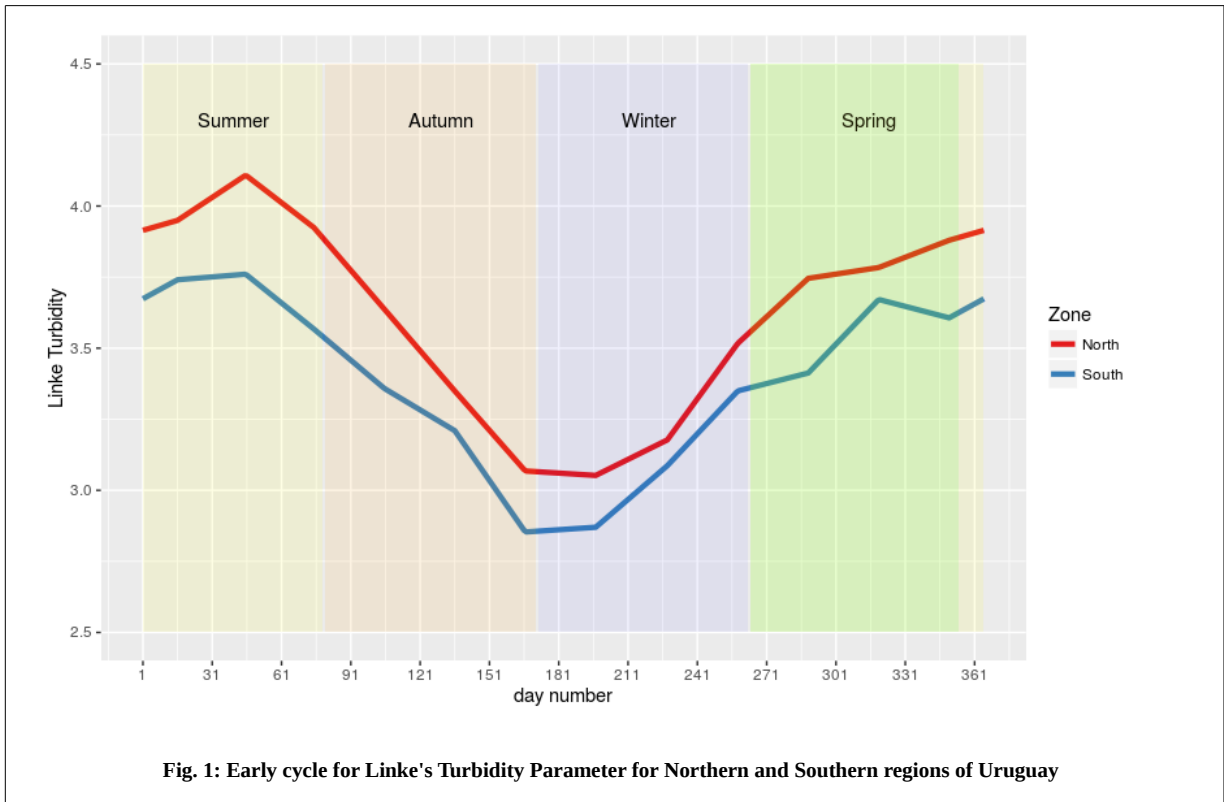
the original SOLIS model (Mueller, 2004) the optical depth τ_g and the parameter g are calculated from a RTM for different sun elevation angles, which limits the real-time applicability of this model. To solve this problem, Ineichen fitted analytical expressions for the parameters involved. Explicit expressions for I_o , τ_g and g as functions of $aod700$, water vapor (w) and atmospheric pressure (p) are provided in (Ineichen 2008). According to this author, the simplification implies a negligible bias and standard deviation of 3 W/m^2 when compared with the results of the original RTM calculation.

2.2 Atmospheric data

Three atmospheric variables (T_L , $aod700$ and w) are used as input for the models described above. For the region of interest in this work ground-based measurements are not available for any of them. However, as they are expected to vary slowly, yearly cycles of daily information based on satellite and ancillary ground data can be used. In the following, this methodology is explained in further detail.

Linke Turbidity

As mentioned before, T_L includes in an effective way information on water vapor content and aerosols in the atmosphere. T_L can be estimated either from (i) water vapor and aerosol optical thickness at different wavelengths (Remund et al., 2003), (ii) from ground-based clear-sky DNI measurements and eq. (1) or (iii) from clear-sky GHI measurements and eqs. (1) and (2) (Diabaté et al., 2003; Raichijk, 2009). When clear-sky DNI is available, (ii) is the preferred method (Pedros et al., 1999; Raichijk y Fasulo, 2010; Remund et al., 2003). For the region of interest in this work, this is not the case and it is necessary to resort to methods based on GHI data. The alternative of using parametric models to estimate the diffuse fraction from GHI and then use method (ii) mentioned above to obtain T_L from DNI has been used by (Cucumo et al., 2000) but the high uncertainty introduced by the DNI estimation procedure (Abal, 2017) render this method unreliable.



In this work, we use the method (iii), to estimate daily T_L at several locations in the region of interest. T_L is determined in order to get the best fit of the ESRA model against clear-sky GHI ground data for ten different locations in the region that includes Uruguay and neighbouring areas (Laguarda and Abal,

2016). Clear sky hourly data were selected from the 2010-2015 period using the procedure described in (Remund et al., 2003). Then, the monthly-averaged T_L was chosen in order to minimize a statistical indicator Kolmogorov Smirnov Index, KSI). The monthly values of T_L and their uncertainty was determined using a standard 10-fold cross validation technique. The data set used to obtain the T_L cycles is independent of the data used in this work for the evaluation of the clear sky models. This method was validated against the DNI-based method for a few locations where DNI measurements were available, for details we refer to (Laguada and Abal, 2016). A daily T_L cycle is constructed by linear interpolation of the monthly mean values. Since the observed spatial dependence of this cycle is weak, just three daily-interpolated cycles (for the northern (N), center (C) and southern (S) parts of the country) adequately describe average atmospheric conditions at all sites. The T_L cycles used in this work (Northern and Southern regions) are shown in Fig. 1.

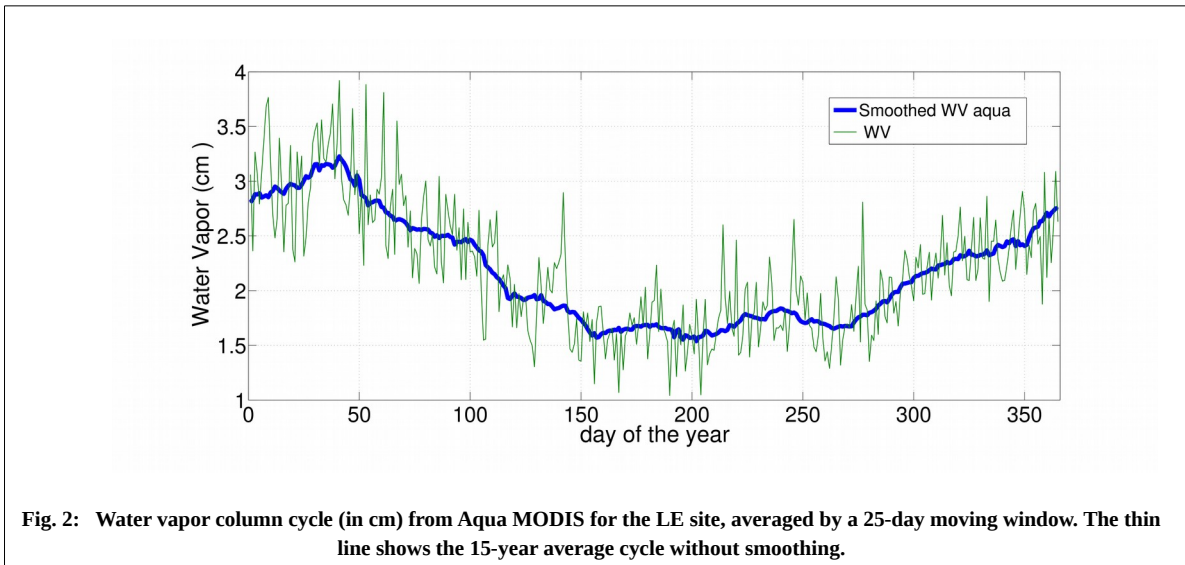
Aerosol Optical Depth and Water Vapor

The sSOLIS model describes the atmosphere using only aod700 and water vapor density as required information. Since there are no Aeronet or similar specialized measuring sites for these magnitudes in Uruguay, MODIS daily satellite estimates for water vapor column, Angstrom exponent and aod550 for 15 years (2/2002 to 12/2016) were used to estimate yearly cycles of the atmospheric variables. The Angstrom relation is used to obtain aod700 from aod550,

$$\tau_{700} = \tau_{550} \left(\frac{700}{550} \right)^\alpha \quad (5)$$

where α is the Angstrom exponent. Yearly cycles of average water vapor and aod700 were generated to be used as input for the sSOLIS model. The long term Aqua-MODIS satellite time series (area-averaged) data was used. The data is downloaded from the NASA site <https://giovanni.gsfc.nasa.gov/giovanni/>, and belongs to the level 3 series (highest quality available).

Specifically, daily information of Aerosol Angstrom coefficient (α), aod550, and precipitable water vapor column (w) from 2002 to 2015 were used for each site of interest. Using eq. (5), a series for aod700 series was obtained for each site. The final smoothed aod700 and w yearly cycles are obtained by averaging the series for each day of the year, and then taking a 25-day moving average and excluding data that exceeds 2 times the standard deviation for each day. The resulting smoothed cycles and the 15-year average cycles for w and aod700 at a given site are shown in Figs. 2 and 3, respectively.



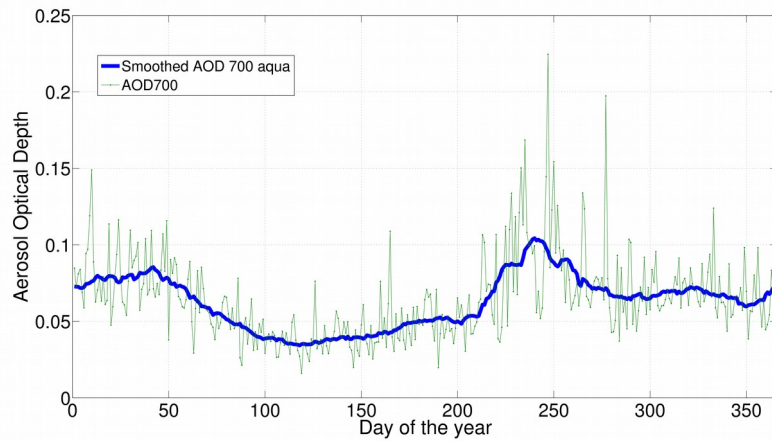


Fig. 3: Aerosol Optical Depth (dimensionless) yearly cycle from Aqua MODIS for the LE, averaged by a 25-day moving window. The thin line shows the 15-year average aod700 without smooting.

2.3 Ground solar irradiance data

The hourly irradiance predicted by these three models are compared with more than two years (January 2015 – March 2017) of GHI ground data from five sites from the continuous solar irradiance monitoring network run by our laboratory (see Table 1 and Fig. 4) GHI is registered each minute with first class or better pyranometers which are calibrated every two years at our laboratory against a Kipp & Zonen CMP22 secondary standard. This calibration is trazable to the PMOD World Radiation Center primary standard and to the World Radiometric Reference. All sites are in rural or semi-rural areas at low altitudes (less than 140 meters above the sea level) in a temperate climate.

Table 1: Details for the ground stations. The clear sky hours correspond to the data filtered and selected in the period january 2015 - March 2017 in all locations.

| Site Code | Zone code | Latitude South degrees | Longitude West degrees | Altitude (m. a. s. l.) | Valid daytime hours | Clear Sky hours |
|--------------|-----------|------------------------|------------------------|------------------------|---------------------|-----------------|
| LB | S | 34.67 | 56.34 | 37 | 8985 | 3105 |
| AR | N | 30.40 | 56.51 | 136 | 9832 | 3218 |
| LE | N | 31.27 | 57.89 | 50 | 6147 | 1958 |
| TT | S | 33.28 | 54.17 | 35 | 6854 | 1840 |
| RC | S | 34.49 | 54.31 | 20 | 8676 | 2496 |
| Total | - | - | - | - | 40494 | 12617 |

Clear-sky filtering procedure

The ground data is filtered for basic quality control and integrated to obtain 40494 (daytime) valid hourly records. In order to obtain data associated to clear sky conditions, the algorithm in (Remund et al. 2003) is used to select 12617 (mostly) clear-sky hours. This algorithm is based in apply five consecutive filters to GHI hourly data.

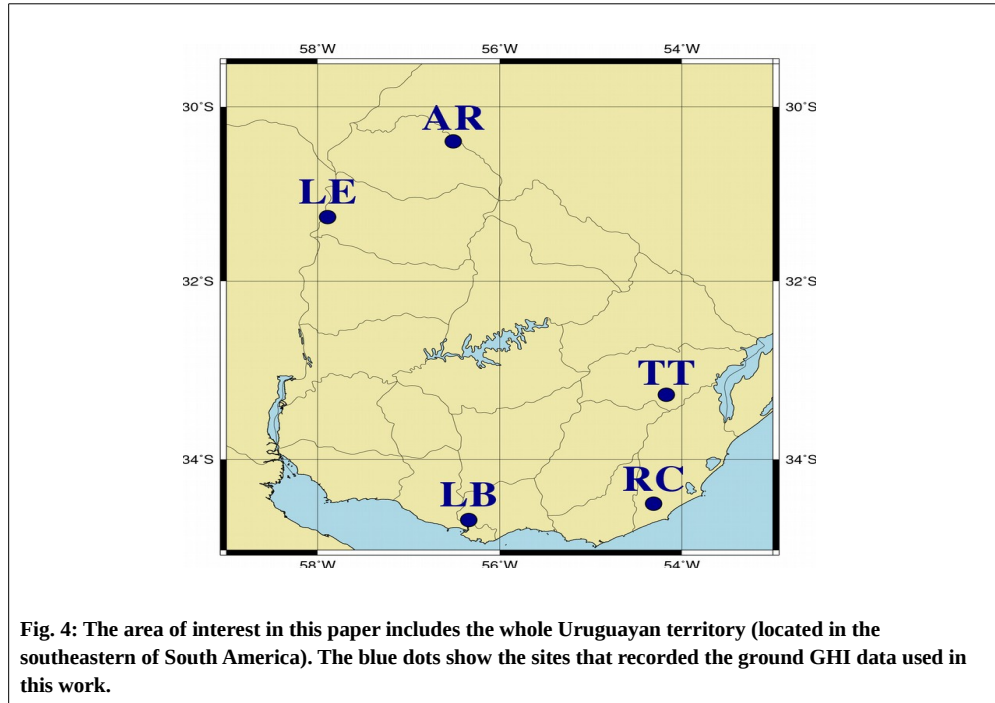
1. $DNI < 200 \text{ W/m}^2$. If DNI simultaneous information isn't available, it is estimated using Erbs correlation (Erbs et al., 1982). This procedure is only approximate, but it is sufficient to discriminate low direct radiation hours.
2. The hourly modified clearness index k_t' (Perez et al., 1990), Ec. (6), must be lower than 0.7 (Molineaux and Delaunay, 1995).

$$k_t' = \frac{k_t}{0.1 + 1.031 e^{-\frac{1.4m}{9.4 + 0.9m}}} \quad (6)$$

where $k_t = I_h / I_0$ is the usual clearness index, and m is the air mass.

3. The daily clearness index ($K_t = H_h / H_0$) must be over 0.4.
4. For a given day if the clear sky hours are less than the 40% of the valid hours, then the whole day is discarded.
5. Data with solar zenith angle below 10 degrees is discarded.

After this set of five filters is applied, a set of clear sky hours is obtained for each site. The last column of Table 1 shows the number of hours for each site. These data was used as indicated in Section 2.2 to obtain monthly averaged T_L values for each site. Since site-to-site variability is low, data was grouped in three regions (North, Middle and South) and monthly T_L cycles for each region were obtained. These average cycles were interpolated linearly to obtain daily data and avoid abrupt changes across consecutive months.



In (Laguarda and Abal, 2016) the ESRA model with these T_L cycles was compared to hourly clear sky data from 8 sites and the relative Root Mean Square Deviation (RMSD) was between 4.1 % and 5.1 % for all sites. These results show that clear-sky GHI can be estimated in this region by the ESRA model with

uncertainty under 5 % using the mean T_L cycle determined for a broad region from long-term data. Marginal improvements (under 1 %) can be obtained by using specific T_L cycles for each site.

3. Model performance

Three indicators used to evaluate model performance are Mean Bias Deviation (MBD), Root Mean Square Deviation (RMSD) and the Kolmogorov-Smirnov Integral (KSI). They measure bias, spread and distance between statistical distributions, respectively. Their definitions are standard and can be found in Appendix A. Table 2 lists these indicators for each clear-sky model and site. All models have small negative bias (indicating a tendency to underestimate GHI). Typical RMSD value range between 4 % and 7 %, depending on site and model.

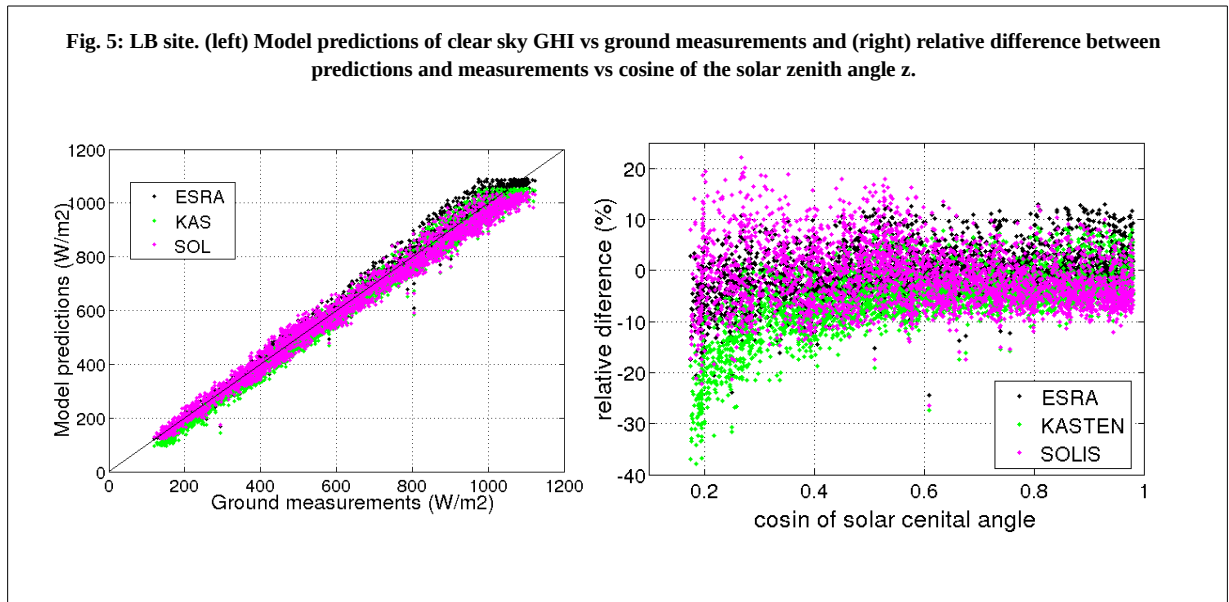
| Site | Mean | ESRA | | | KIP | | | sSOLIS | | |
|------------|-------------------|-------------|------------|------------|-------------|------------|------------|-------------|------------|------------|
| Code | Wh/m ² | MBD | RMSD | KSI | MBD | RMSD | KSI | MBD | RMSD | KSI |
| LB | 615 | 0.0 | 4.3 | 1.1 | -4.4 | 6.1 | 4.4 | -2.3 | 6.0 | 2.7 |
| AR | 629 | -0.6 | 4.3 | 1.1 | -5.0 | 6.5 | 5.0 | -2.1 | 5.5 | 2.1 |
| LE | 662 | -0.3 | 3.8 | 0.9 | -4.5 | 5.9 | 4.5 | -3.4 | 5.9 | 3.4 |
| TT | 589 | -0.8 | 4.8 | 1.0 | -5.2 | 7.0 | 5.2 | -2.0 | 6.2 | 2.4 |
| RC | 616 | -1.0 | 4.7 | 1.2 | -5.3 | 7.0 | 5.3 | -2.3 | 6.2 | 2.8 |
| ALL | 622 | -0.5 | 4.4 | 1.1 | -4.9 | 6.5 | 4.9 | -2.4 | 6.0 | 2.7 |

A simple global indicator C can be constructed for each model by averaging the absolute bias with RMSD and KSI (Gueymard 2014, Abal et al, 2017). This indicator, shown in Table 3, suggests that ESRA is the best model, followed by sSOLIS.

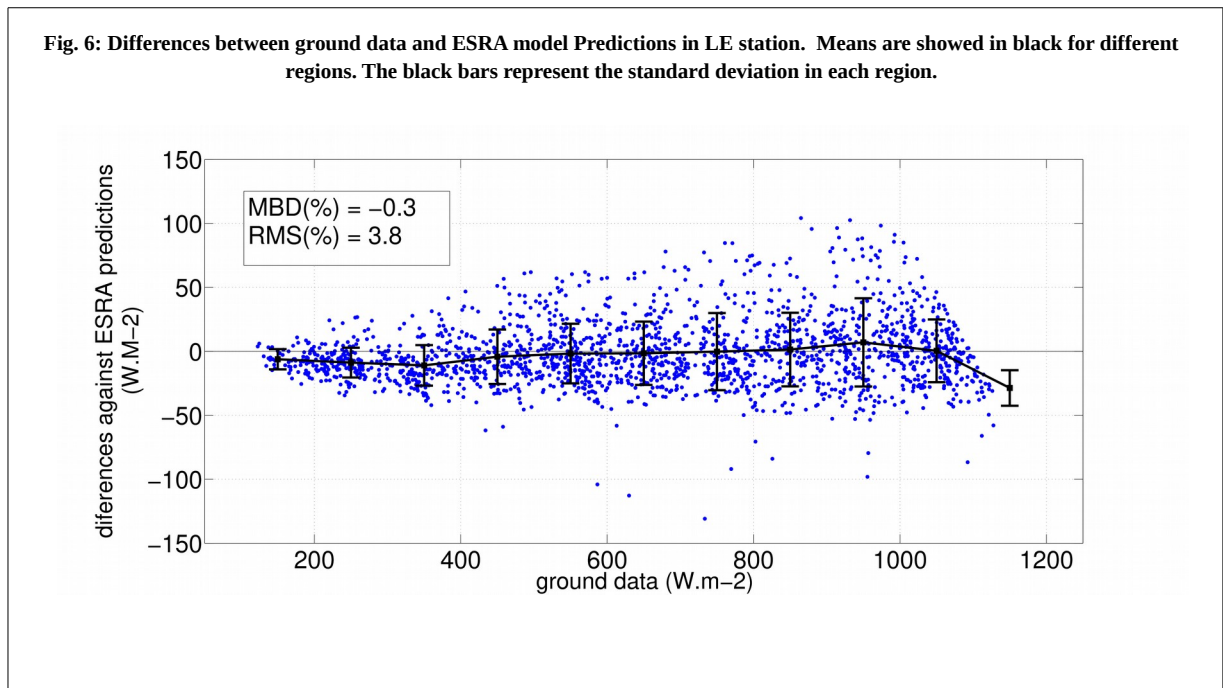
| Model | $C = (MBD + RMSD + KSI) / 3$ |
|--------|--------------------------------|
| ESRA | 2.0 |
| KIP | 5.4 |
| sSOLIS | 3.7 |

Fig. 5 shows detailed results for the LE site. The Left panel compares model prediction with ground measurements. The small negative bias (underestimation) is associated to high irradiance ($> 700 \text{ W/m}^2$) conditions. The right panel shows relative differences vs cosine of zenith angle. For low cosine values (low solar altitude) the biases increase as expected. The KIP model has a particularly large bias under this conditions. Fig. 6 shows the absolute difference between the ESRA model prediction and the ground truth vs Irradiation value. GHI values were classified into 11 bins, and average and standard deviation for each bin was calculated. This shows that bias is under 25 W/m^2 in all cases. For this model, negative biases come mainly from low irradiance ($< 400 \text{ W/m}^2$) values. Since we are considering clear-sky data, these values are associated to low solar altitudes for which measurements are most uncertain.

Part of the observed deviations may be due to error in measurement or to errors in the automated clear-sky algorithm classification (i.e. mostly clear hours classified as cloudy or partly cloudy hours classified as clear). This can only be assessed by a manual selection of the clear sky hours, a daunting task for the amount of data considered in this work.



These results are similar to those found in the literature for these models. In (Ineichen, 2006) data from 16 sites in the Northern Hemisphere (with latitudes ranging between 30 and 48 degrees) was used to compare the performance of eight clear-sky models. Among them, the SOLIS model (the simplified model was not introduced until 2008), the ESRA and the KIP models. The SOLIS model was found to be one of the best among the models considered. Another comprehensive comparison was performed in (Gueymard, 2012) using high quality data from five sites in the Northern Hemisphere (latitudes between 19.5 and 40 degrees).



Tab. 4: A comparison of indicators for the selected models

| Model | Indicator | (Gueymard, 2012) | (Ineichen, 2006) | This work |
|-----------------------------------|------------------|-------------------------|-------------------------|------------------|
| ESRA | MBD (%) | 3.1 | 4.0 | -0.5 |
| | RMSD (%) | 4.5 | 6.0 | 4.4 |
| KIP | MBD (%) | not tested | -0.2 | -4.9 |
| | RMSD (%) | not tested | 4.6 | 6.5 |
| sSOLIS | MBD (%) | -1.6 | (*) 1.8 | -2.4 |
| | RMSD (%) | 2.8 | (*) 4.9 | 6.0 |
| Mean GHI (w/m²) | | 675.6 | 547.0 | 622.0 |

(*) indicators are for the original SOLIS model.

In this comprehensive comparison, 18 clear-sky models were considered (the KIP model was not among them). The ESRA and simplified SOLIS were included and in fact, the sSOLIS was found to be the second best model, after the REST2 model.

It is not always possible to compare results from different authors, but in these cases, enough information is given so that results for all sites can be reduced to the same form and their averages are compared in Table 4. The relative RMSD indicators are similar in the three studies, ranging between 3% and 6% of the mean. As noted in (Ineichen, 2006) since there are no large differences in performance, the best clear sky model for a given region and application should be chosen with consideration to implementation simplicity and with regard to the quality and availability of its input data. For instance, in this study ESRA outperforms the sSOLIS model, which was found to be the second best among 18 other models in (Gueymard 2012). However, this study used the best available data for water vapor and aod, while in our implementation we have used daily averages based on satellite retrievals, which is available for this region. So, model rankings should not be read as ranking models according to their accuracy, but rather as ranking local model implementations (which include the quality of their input data).

4. Summary and conclusions

Three simple clear sky models (ESRA, Simplified SOLIS (sSOLIS) and Kasten (KIP)), are considered and evaluated using data for the region of Uruguay and neighboring areas (southeastern South America). These models have been selected taking into account the availability of the required input information for this area. Two of them use Linke Turbidity as their single parameter and sSOLIS uses water vapor density and Aerosol Optical Depth at 700 nm. This information was obtained from the MODIS satellite database on a daily basis and averaged over 15 years. The average Linke Turbidity was obtained from a large set of clear-sky GHI data for 10 sites on the region of interest by minimization of the KSI index.

The models are evaluated against an independent data set (i.e. not used to determine the TL cycles) from five sites in the region of interest. Clear sky conditions are automatically selected based on a set of criteria suggested by Remund, in which the Perez modified clearness index plays an important role. Results show that all models have RMSD between 4.3 % and 7 % of the mean value of GHI. Mean Bias is mostly negative for all models and sites, reaching -5.3%.

Our first conclusion is that our implementation of the ESRA model has the best indicators over all sites considered in this work. A combined indicator selects this model as the best alternative to estimate clear-sky GHI in this region. Clear-sky GHI can be estimated with bias under 1% and Root Mean Square Deviations under 5 % of the mean. In absolute terms, averaged over sites, the bias is $MBD = -3 \text{ W/m}^2$ and the

RMSD = 27 W/m². These indicators can be improved if T_L information for specific sites is used in the ESRA model. However, the implementation based on the average cycle has indicators that are low enough to allow the use of the ESRA model in automated quality-check procedures for the ground GHI data. Furthermore, it is an adequate starting point for a physically motivated all sky irradiation model in which information about cloudiness is obtained from satellite images.

A second conclusion is that, since there are no drastic variations in performance, the selection of a clear sky model should take into account its ease of implementation and the quality and availability of its input data.

5. References

- Abal, G., Aicardi, D., Alonso-Suárez, R., 2017. Performance of empirical models for diffuse fraction in Uruguay. *Solar Energy*, 141, 166-181.
- Cano, D. Et al. 1986. A method for the determination of the global solar radiation from meteorological satellite data, *Solar Energy*, 37, 31–39.
- Cucumo, M., Kaliakatsos, D., Marinelli, V., 2000. A calculation method for the estimation of the Linke turbidity factor, *Solar Energy* 19, 249-258.
- Diabaté, L., Remund, J., Wald, L., 2003. Linke turbidity factors for several sites in Africa. *Solar Energy* 75, 111-119.
- Erbs, D., Klein, S., Duffie, J., 1982. Estimation of the diffuse radiation fraction for hourly, daily and monthly average global radiation. *Sol. Energy* 28, 293.
- Grenier, J.C. et al., 1994. A spectral model of Linke's turbidity factor and its experimental implications. *Solar Energy*, 52, 303-313.
- Gueymard, C.A., 2008. REST2: High-performance solar radiation model for cloudless-sky irradiance, illuminance, and photosynthetically active radiation, *Solar Energy* 82, 272–285.
- Gueymard, C. 2012. Clear-sky irradiance predictions for solar resource mapping and large-scale applications: improved validation methodology and detailed performance analysis of 18 broadband radiative models. *Solar Energy* 86, 2145-2169.
- Gueymard, C., 2014. *Renew. Sustain. Energy Rev.* 39, 1024.
- Ineichen, P., 2008. A broadband simplified version of the Solis clear sky model. *Solar Energy* 82, 758–762.
- Ineichen, P., Perez, R., 2002. A new airmass independent formulation for the Linke Turbidity coefficient, *Solar Energy* 73, 151-157.
- Ineichen, P. 2006. Comparison of eight clear sky broadband models against 16 independent data banks. *Solar Energy* 80, 468-478.
- Kasten, F., 1996. The linke turbidity factor based on improved values of the integral rayleigh optical thickness. *Sol. Energy* 56, 239–244.
- Laguarda, A., Abal, G., 2016. Proceedings of XXXIX ASADES, La Plata, Argentina, Oct. 2016. Available at https://www.fing.edu.uy/~abal/trabajos/TL_asades_201608_final.pdf.
- Louche, A. et al. 1986. An analysis of the Linke turbidity factor. *Solar Energy* 37, 393-396.
- Mavromatakis F. and Franghiadakis, Y., 2007. Direct and indirect determination of the Linke turbidity coefficient. *Solar Energy* 81, 896-903.
- Molineaux, B., Delaunay, J.J., 1995. Direct luminous efficacy and atmospheric improving model performance 55, 125–137.

- Mueller, R. et al., 2004. Rethinking satellite based solar irradiance modelling – the SOLIS clear-sky module. *Remote Sens. Environ.* 91, 160-174.
- Pedrós, R., Utrillas, M.P., Martínez-Lozano, J.A., Tena, F., 1999. Values Of Broad Band Turbidity Coefficients In A Mediterranean Coastal Site, *Solar Energy* 66, 11-20.
- Perez, R., Schlemmer, J., Hemker, K., Kivalov, S., Kankiewicz, A., and Gueymard, C. (2015). Satellite-to-irradiance modeling - a new version of the SUNY model. *IEEE 42nd Photovoltaic Specialist Conference (PVSC)*, pages 1–7.
- Perez, R., Ineichen, P., Moore, K., Kmiecik, M., Chain, C., George, R., and Vignola, F. (2002). A new operational model for satellite-derived irradiances: description and validation. *Solar Energy*, 73, 307–317.
- Perez, R., Ineichen, P., Seals, R., Zelenka, A., 1990. Making full use of the clearness index for parameterizing hourly insolation conditions. *Sol. Energy* 1, 3–6.
- Raichijk, C., (2009). Estimación del índice de turbidez de linke para distintas localidades de Argentina, *Avances en Energías Renovables y Medio Ambiente (AVERMA)*, 13, pp. 11-16.
- Raichijk, C., Fasulo, A., (2010). Estudio de la turbidez atmosférica en la ciudad de San Luis, *Avances en Energías Renovables y Medio Ambiente (AVERMA)*, vol. 25.
- Remund, J., et al., 2003. Worldwide Linke turbidity information. In: *Proceedings of ISES Conference*. Stockholm, Sweden, International Solar Energy Society.
- Reno, M.J., Hansen, C.W., Stein, J.S., 2012, Global Horizontal Clear Sky Irradiance: implementation and analysis. SANDIA REPORT SAND2012-2389.
- Rigollier, C., Lefevre, M., and Wald, L. (2004). The method Heliosat-2 for deriving shortwave solar radiation from satellite images. *Solar Energy*, 77, 159–169.
- Rigollier, C., Bauer, O., Wald, L., 2000. On the clearsky model of the 4th ESRA with respect to the heliosat method. *Solar Energy* 68, 33-48.
- Spencer, J.W (1971). Fourier series representation of the position of the sun. *Search*, 2:172, 1971.

5. Appendix: Statistical indicators

There are several concordance indicators between measurements \hat{Y}_i , and n estimates Y_i of a variable. In this section RMSD, MBD, and KSI are defined.

The root mean square deviation (RMSD), and de Mean Bias Deviation (MBD) are defined as

$$RMSD = \sqrt{\frac{1}{n} \sum_{i=1}^n (\hat{Y}_i - Y_i)^2}$$

$$MBD = \frac{1}{n} \sum_{i=1}^n \hat{Y}_i - Y_i$$

For a variable z, the the Kolmogorov-Smirnov Integral indicator (KSI) is defined as

$$KSI = \int_{z_{min}}^{z_{max}} D(z) dz$$

where

$$D(z) = |F_{\hat{Y}}(z) - F_Y(z)|$$

Here F_Y ($F_{\hat{Y}}$) is the empirical cumulative distribution function (CDF) for the variable Y (\hat{Y}), were Y and \hat{Y} the measurements and model estimated data vectors of GHI, z is variable in the range of GHI. In this case, KSI (same units as GHI, W/m²) is a measurements of the absolute difference between the CDFs.

Each statistical indicator can be expressed in a dimensionless way as

$$rMBD = \frac{RMBD}{mean(\hat{Y})}$$

and similar relations for the other indicators.

